MOEM

Modern Electronic Materials 2019; 5(2): 77–85
DOI 10.3897/j.moem.5.2.51365

Research Article

Physicochemical fundamentals of phase formation in silicon layers implanted with oxygen and carbon

Andrey N. Aleshin[1], Kira L. Enisherlova[2]

1 Institute for Ultrahigh Frequency Semiconductor Electronics, Russian Academy of Sciences, 7/5 Nagorny Proezd, Moscow 117105, Rusia
2 J&C «S&PE «Pulsar», 27 Okruzhnoy Proezd, Moscow 105187, Russia

Corresponding author: Kira L. Enisherlova (enisherlova@pulsarnpp.ru)

Received 17 February 2019 ♦ **Accepted** 11 May 2019 ♦ **Published** 1 June 2019

Citation: Aleshin AN, Enisherlova KL (2019) Physicochemical fundamentals of phase formation in silicon layers implanted with oxygen and carbon. Modern Electronic Materials 5(2): 77–85. https://doi.org/10.3897/j.moem.5.2.51365

Abstract

The thermodynamic and kinetic regularities of processes occurring during heat treatment in silicon layers implanted with oxygen and carbon ions have been considered. We have analyzed the regularities of silicon deformation, impurity distribution and defect formation after different annealing modes. Diffusion smearing of implanted impurities in these layers has not been observed during carbon and oxygen implantation. As-annealed carbon does not occupy sites of the silicon lattice, in contrast to the implantation behavior of other impurities, e.g. boron and phosphorus. Phase formation regularities in implanted layers during subsequent heat treatment have been analyzed. Changes in the free energy of the system during heterogeneous and homogeneous precipitate nucleation have been compared. Sequential implantation with carbon and oxygen ions has been found to initiate diffusion flows of carbon and oxygen toward the center of the ion doped layer (the uphill diffusion phenomenon). The possibility of uphill diffusion has been analyzed from the standpoints of the Onsager theory. We show that the contribution of the chemical interaction between oxygen and carbon is far greater than the entropy contribution to the diffusion flux. We have demonstrated the high efficiency of ion doping with oxygen and carbon for gettering of uncontrolled impurities from active regions of silicon structures. The efficiency of this gettering process has been assessed for epitaxial structures in which layers had been grown on silicon wafers implanted with these impurities. Uphill diffusion in the layers after double doping with carbon and oxygen has led to the formation of more defects which may provide for efficient gettering. We have found the optimal oxygen and carbon implantation dose ratio for maximal gettering efficiency.

Keywords

semiconductors, ion implantation, silicon, defect formation, gettering, gettering centers, diffusion smearing, uphill diffusion

1. Introduction

One of the problems solved with the help of advanced semiconductor technologies, e.g. ion implantation is the synthesis of metastable nanosized heterophase structures in a semiconductor matrix. These structures can be synthesized primarily through the formation of binary compositions if the implanted component is an insoluble or low soluble element, e.g. carbon. By choosing implantation temperature and carbon ion flux intensity and making use of impurity coagulation in the matrix, e.g. in copper or silver, one can produce nanosized carbon particles, the so-called carbon onions having a fullerene structure [1–3]. These nanosized carbon particles produce local elastic stress fields around themselves and thus can become active gettering centers. Carbon has a low solubi-

lity in silicon and can therefore be considered as an ion implanted getter. Typically ion implantation is performed at room temperature thus forming a supersaturated Si–C solid solution which then decomposes during heat treatment. Carbon has the same valence as silicon, and this eliminates the problem of layers with detrimental charged centers that form during annealing.

The method of gettering by means of ion implantation of usually light elements (C, He, O) when the getering regions are located as close as possible to active device structures is well known as proximity gettering [4, 5]. This approach is technologically adaptable as it can be easily integrated into device fabrication cycles by separating ion implantation and subsequent annealing which can be coupled with device heat treatments. This getter formation method is the most efficient for silicon devices the active regions of which form in epitaxial layers, e.g. for bipolar transistors and ICs on their basis as well as for several types of matrices and lines of **CCD** (charge coupled device) structures. However as was shown in [6] to achieve gettering by implanting solely carbon ions it is needed to employ high energy process (of the order of MeV) with a large dose of implantation (a dose of 10^{16} 1/cm^2) which complicates the technology. As shown earlier [7, 8] implantation of two impurities (oxygen and carbon) at low doses may be more efficient since the presence of strong chemical bond between these impurities changes phase formation processes in ion doped layers.

The aim of this work is to generalize all experimental data on phase formation during heat treatment and regularities of diffusion observed in silicon layers implanted with carbon, oxygen and jointly with oxygen and carbon, and to describe the thermodynamics and kinetics of processes occurring in ion doped layers during annealing. Analysis of defect formation processes during annealing of layers implanted with these impurities is also of interest since C and O are the main background impurities in silicon the presence and interaction of which mostly determine the properties of the material. Although ion doped regions are heavily supersaturated, study of phase formation in these layers may provide additional useful information.

2. Experimental

We studied the structure and analyzed the concentration profiles of ion implanted impurities in zone melting grown KEF-20 silicon wafers with (100) working surface orientations. Ion implantation was carried out in dechanneling mode without target heating, at a 300 keV energy and a 0.1 mA ion beam current so as to avoid specimen heating by the ions. At this energy the mean projected ranges R_p of oxygen and carbon ions are almost the same, i.e., 0.68 μm [9]. We performed implantation with solely oxygen ions, with solely carbon ions and also consistent implantation with these ions. The conditions of consistent implantation with two impurities were chosen so the total dose was the same as for implantation with one impurity. The dose was varied from 6×10^{14} to 4.2×10^{15} 1/cm^2 (from 100 to 700 μCl/cm^2). The ion beam scanned the specimen surface so the doping region was in the form of a spot with a 3 cm linear size. To analyze phase formation during subsequent anneals we chose the maximum technologically admissible annealing temperature, i.e., 1200 °C. The specimens were annealed in a technical purity argon flow for 2–7 h, the furnace heating rate before entering the steady state annealing mode being 4 K/min. To avoid the influence of possible oxidation processes the silicon wafer surfaces were preliminarily capped with a 50 nm silicon nitride film. The film was deposited at T = 950 °C for 20 min. The efficiency of gettering was assessed for KES-0.01 silicon wafers the working surfaces of which were implanted with the test impurities. Then we grew a 2 μm film of KEF-0.7 silicon on these surfaces by gas epitaxy at 1200 °C for 1 h. The resultant two-layered structures were additionally annealed in an oxygen environment at 1200 °C for 1 h. Thus the total heat treatment time of the epitaxial structures was 2 h.

The following methods were used in the study:

- to assess the type and degree of deformation in thin surface layers of the as-implanted and as-annealed test specimens we used double-crystal X-ray diffraction, taking the diffraction curves;
- the distributions of the implanted impurities in the as-implanted and as-annealed specimens were studied using secondary ion mass-spectrometry **(SIMS)** on an ISM-3F spectrometer;
- regularities of defect formation were analyzed using transmission electron microscopy **(TEM)**;
- gettering efficiency was evaluated for the epitaxial structures by making spherical cross-sections, etching defects in the surface layers and calculating the density of defects in the epitaxial films.

3. Results and discussion

Analysis of the diffraction curves for the as-implanted specimens showed that all the experimental versions of ion implantation produced elastic stresses in the specimens and deformed their lattice in surface layers, as indicated by additional peaks in the diffraction curves at lower reflection angles. This peak position suggests an increase in the lattice parameter [10]. Similar stresses are observed, for example, in silicon after boron implantation. X-ray studies showed that the regularity of elastic stress behavior with an increase in dose was almost the same for all the versions, i.e., implantation with solely carbon, implantation with solely oxygen and double implantation with these impurities (Fig. 1). With an increase in the dose of implanted ions the number of additional peaks increased suggesting an increase in the deformation. However after annealing at 1200 °C for 2 h the diffraction curves of the specimens implanted with one or two impurities were the same as those of the reference non-implanted specimens.

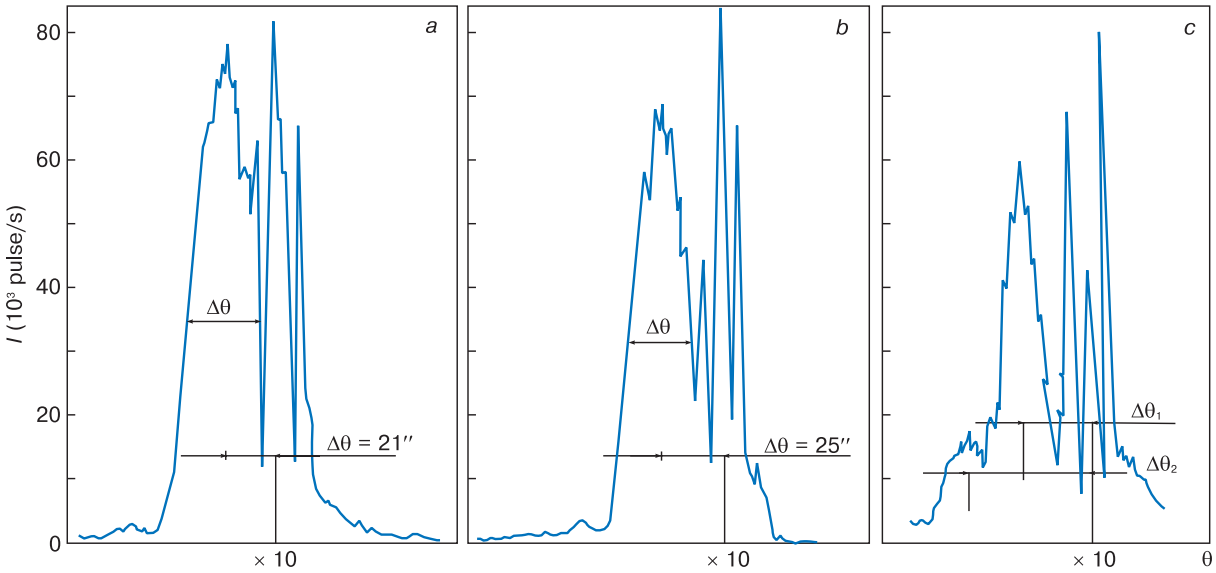

Figure 1. Diffraction curves after ion implantation: (*a*) O^+, dose 6×10^{14} 1/cm^2; (*b*) C^+, 1.2×10^{15} 1/cm^2; (*c*) C^+, 6×10^{14} 1/cm^2 + O^+, 1.8×10^{15} 1/cm^2.

This indicates a complete relief of the stresses and hence suggests that these impurities do not occupy silicon lattice sites after annealing.

Electron microscopic studies expectedly showed that oxygen-silicon precipitates formed in the oxygen implanted layers after annealing at 1200 °C. The precipitates had typical shapes and were surrounded by dislocation loops (precipitate-dislocation complexes) (Fig. 2*a*). Their density was within 10^9 cm^{-3} and the sizes of dislocation loop pile-ups for the maximum oxygen ion dose of $2.4 \cdot 10^{15}$ 1/cm^2 were 0.2–0.3 μm, the precipitate size being 10 nm. After implantation of solely carbon and after double implantation of oxygen and carbon with a carbon to oxygen ion dose ratio of 1 : 1 and annealing we observed planar hexagonal structural features (Fig. 2*b*). The sizes of these hexagonal features ranged from 100 to 200 nm and their density in the ion doped layers was $(1–2) \times 10^{11}$ cm^{-3}. Each planar hexagonal feature was decorated by small hemispherical second phase precipitates which seemed to "hang" on the hexagonal features at both sides. This defect structure is schematically shown in Fig. 2*c*. Second phase precipitates produced a moiré contrast with a periodicity of 4.2 nm in the <111> direction which corresponds to the SiO_2 phase. The precipitate sizes ranged from 20 to 50 nm and their density per one hexagonal defect was from 40 to 100, with the smallest number of precipitates being observed in specimens implanted with solely carbon. Thus the density of the precipitates could reach 10^{13} cm^{-3}.

Changing the oxygen implantation dose to be at least twice the carbon dose caused the formation of a completely different type of structural defects after post-implantation annealing. A system of perfect loops formed (Fig. 3). The density of the loops increased as one approached the middle portion of the ion doped layer (Fig. 3*a–c*). The maximum density of the loops was obtained for a carbon to oxygen

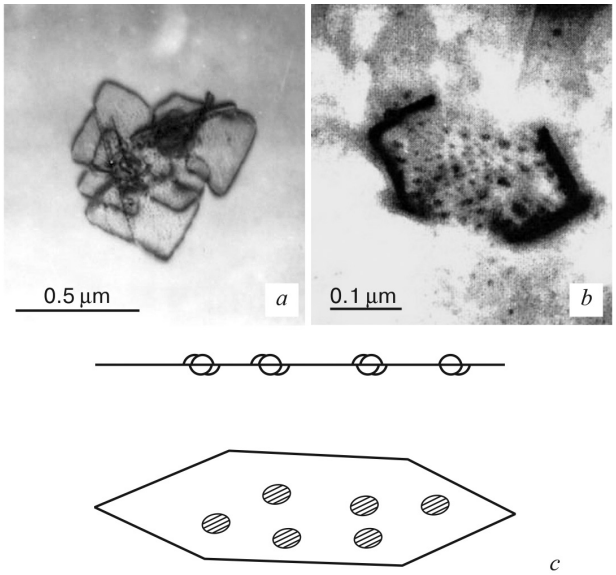

Figure 2. (*a* and *b*) Micrographs of defects in ion implanted silicon layers as-annealed at 1200 °C and (*c*) a schematic of planar defect arrangement in Fig. (*b*): (*a*) O^+, dose 2.4×10^{15} 1/cm^2; (*b*) C^+, 2.1×10^{15} 1/cm^2 + O^+, 6×10^{14} 1/cm^2.

ion dose ratio of 1 : 4. Then the density of the loops in the region close to R_p was ~10^{15} cm^{-3} which is 2 orders of magnitude higher than the density of the oxygen-silicon precipitates that formed on planar hexagonal defects after ion implantation with sole carbon or after double implantation if the oxygen ion dose did not exceed the carbon ion dose.

Study of the implanted impurity concentration profiles in the as-implanted and as-annealed specimens showed that after implantation of one impurity the as-implanted and as-annealed carbon concentration distributions at different implantation doses are generally similar. Their main distinctive feature was that carbon was localized af-

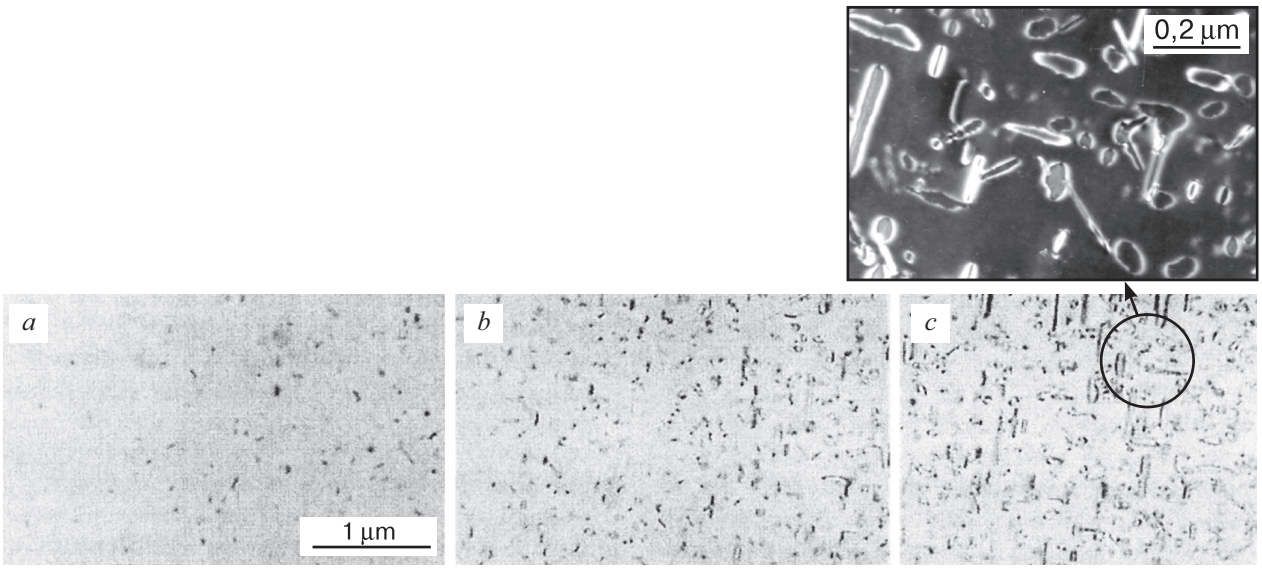

Figure 3. Planar TEM micrograph of silicon surface layer (moving toward the middle of the ion implanted layer, (*a*–*c*)) with interstitial dislocation loops after C and O implantation at a carbon to oxygen dose ratio of 1 : 4 followed by annealing at 1200 °C for 2 h.

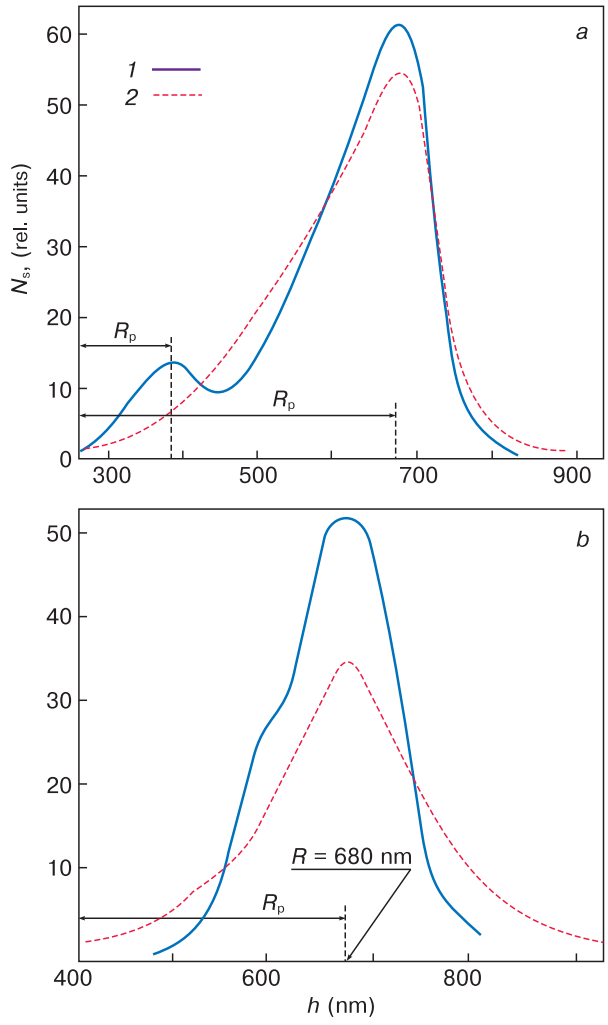

Figure 4. Secondary C ion depth profiles for implanted Si layers (*1*) before and (*2*) after annealing at 1200 °C for 4 h: (*a*) C^+, dose 3.0×10^{15} 1/cm^2; (*b*) C^+, 6×10^{14} 1/cm^2 + O^+, 2.4×10^{15} 1/cm^2.

ter annealing in the same spatial regions as before annealing (Fig. 4*a*). The as-annealed carbon profile had a second additional peak located closer to the wafer surfaces. Furthermore, in the R_p region the main as-annealed carbon concentration peak was higher than the as-implanted carbon concentration. For implantation of two impurities the as-annealed carbon and oxygen concentration distributions changed dramatically (Fig. 4*b*). The main distinctive feature of these concentration profiles was that the as-annealed carbon concentration in the R_p region increased. This suggests that carbon atoms trigger an uphill diffusion mechanism. The most intense carbon uphill diffusion was observed for sequential implantation of carbon and oxygen at doses of 6×10^{14} and $2{,}4 \times 10^{15}$ 1/cm^2, respectively, i.e., for a carbon to oxygen ion dose ratio of 1 : 4 (Fig. 5). The carbon concentration increased simultaneously with the increase in the oxygen concentration, i.e., the carbon and oxygen diffusion fluxes correlated in the bulk. Furthermore, unlike implantation of solely carbon ions, uphill diffusion covers the entire spatial region of implantation after double ion doping.

The main requirements to gettering regions which attract detrimental impurities during heat treatment are as follows:

– stability of spatial dimensions during subsequent heat treatments, i.e., minimum smearing of the ion doped regions during further growth of epitaxial films and device heat treatments, because otherwise there will be the risk of defect propagation to active device regions due to their proximity;
– presence of gettering centers in these regions capable of trapping and pinning uncontrolled metallic impurities. As was shown earlier, the strongest gettering centers are dislocation fragments [11].

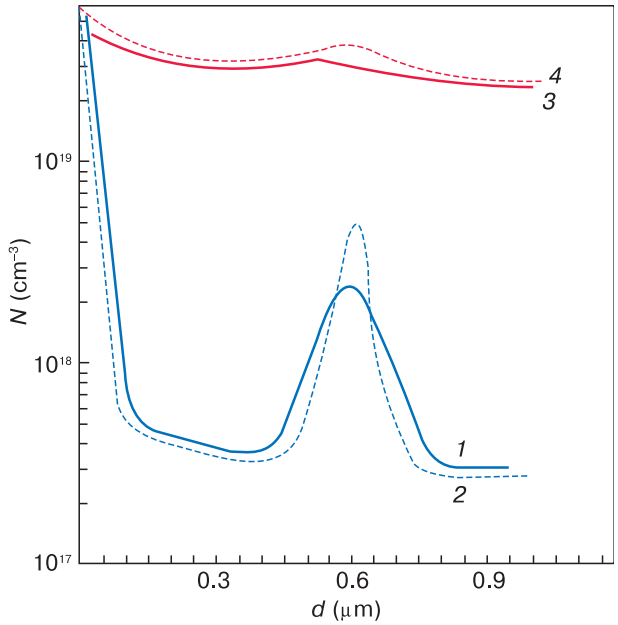

Figure 5. (*1* and *2*) C and (*3* and *4*) O depth profiles in the implanted layer (*1* and *3*) before and (*2* and *4*) after annealing at 1200 °C for 2 h. Carbon ion dose 6×10^{14} 1/cm^2 oxygen ion dose 2.4×10^{15} 1/cm^2.

3.1 Implantation of solely carbon ions

It is believed that growth carbon in single crystal silicon occupies silicon lattice sites. For the temperature in question (T = 1200 °C) the carbon diffusion coefficient is $D_C = (3.5 \div 4.86) \times 10^{-11}$ cm^2/s, its solubility being $c^s_C = 5.4 \times 10^{16}$ cm^{-3} [12]. Thus carbon should be extremely stable against diffusion degradation processes which is favorable for gettering. Analysis of the evolution of the implanted impurity concentration profiles after annealing obtained by SIMS confirmed that the carbon implanted layers did not undergo diffusion smearing (the main peak of the as-annealed carbon concentration profiles was at the same depth as R_p). The as-annealed carbon concentration in that region was even somewhat higher than the as-implanted carbon concentration (Fig. 4*a*). The second carbon concentration peak produced by heat treatment located at ~400 nm (Fig. 4*a*) was most likely caused by trapping of carbon atoms by vacancies close to the surface. (Implantation induced vacancies and interstitial silicon atoms are known to locate in different spatial regions of the silicon matrix: vacancies concentrate closer to the surface while interstitial atoms accumulate at depths greater than R_p [13]). However experiments showed that carbon does not occupy silicon lattice sites after annealing. This was indicated by the absence of additional peaks in the X-ray diffraction curves after annealing. This behavior of implanted carbon differs from that of implanted boron most atoms of which occupy silicon lattice sites after annealing [14, 15] leading to the formation of lattice stresses due to the difference in the ion radii of boron and silicon [16]. But if carbon is in interstitial positions it should have a much higher diffusion rate than that for a vacancy

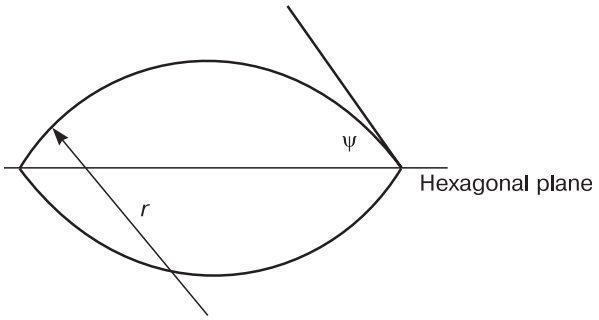

Figure 6. Two hemispeheres of SiO_2 precipitates growing at the walls of planar defects. Ψ is the contact angle and r is the hemisphere radius.

mechanism [12]. This however is not in agreement with experimental results for carbon ion doped layer profiles. The origin of this discrepancy can be clarified by TEM examination of defects in ion doped layers and studies of carbon diffusion after double doping.

Electron microscopic studies showed that the regularities of defect formation in oxygen and carbon implanted silicon layers during post-implantation annealing differ dramatically from those of defect formation in layers implanted with conventional impurities, e.g. phosphorus and boron. After boron and phosphorus implantation at the same total doses annealing causes the formation of dislocation loops, mainly interstitial type ones [14, 15]. In our experiments single ion doping with either oxygen or carbon did not produce loops that form as a result of the coagulation of interstitial silicon atoms during annealing. However heat treatment induced relaxation occurred by different mechanisms for carbon and oxygen implantation. Oxygen atoms that could not diffuse from the ion implanted layer formed standard precipitates with oxygen that were surrounded by dislocation loops (Fig. 2*a*) while carbon occupied lattice sites and formed planar hexagonal structures (Fig. 2*b*, *c*). The contrast observed at different defect plane tilting relative to the electron beam suggests that this defect produced stronger elastic stress fields compared with those of similarly sized standard stacking faults. Thus one can assume that this defect was formed by atoms differing in size from the matrix ones. Furthermore the change in the contrast due to specimen tilting suggests the presence of elastic stress fields forming in the silicon matrix when there is an extra plane embedded in the silicon lattice. One can therefore conclude that the hexagonal features are planar agglomerations of carbon atoms located in lattice pores parallel to the {111} planes. From the structural viewpoint these carbon atom agglomerations are similar to stacking faults.

Planar carbon interlayers evolved into centers of predominant formation of oxygen-silicon precipitates by a heterogeneous mechanism (“hanging” hemispheres in Fig. 2*b*, *c*). This precipitate nucleation mechanism is pos-

sible due to the interaction between carbon and oxygen atoms. Solute oxygen in silicon was attracted to carbon interlayers which locate, as shown above, mainly near R_p and participated in the formation of oxygen-silicon precipitates. Thus a diffusion flux of oxygen atoms was directed from the peripheral regions of the ion implanted layer toward the center of the carbon distribution profile, tending to compensate the oxygen loss caused by the precipitate nucleation. The chemical interaction between carbon and oxygen atoms also attracted carbon to the center of its concentration profile. This latter process led to the observed slight growth of the as-annealed carbon concentration near R_p (Fig. 4*a*). One can indirectly estimate the strength of the carbon-oxygen bond for heterogeneous precipitate nucleation on planar hexagonal carbon interlayers by comparing the change in the Gibbs free energy of the system between two precipitate nucleation mechanisms, i.e., the heterogeneous and homogeneous ones. For the heterogeneous precipitate nucleation on hexagonal interlayers considered herein the shapes of the precipitates are not spherical, and the deviation from a spherical shape can be described with the contact angle Ψ (Fig. 6). The number of precipitates N per unit area of the interface is described as follows [17]:

$$N = \frac{N_0}{x_\theta}\exp\left(-\frac{\Delta G^*}{kT_{\text{nucl}}}\right), \tag{1}$$

where x_θ is the oxygen concentration in SiO_2 expressed in atomic fractions, ΔG^* is the work of nucleation per unit precipitate, N_0 is the number of potential precipitate nucleation sites per unit area of the interface, k is the Boltzmann constant and T_{nucl} is the nucleation temperature. ΔG^* depends on the change in the free Gibbs free energy ΔG_V per unit volume of growing precipitate, the interphase surface tension $\sigma_{\alpha\theta}$ between silicon and precipitates (hereinafter the α and θ phases, respectively) and the contact angle Ψ. The correlation between ΔG^* and ΔG_V is described by the expression [17]

$$\Delta G^* = \frac{4\pi\sigma_{\alpha\theta}^3}{3\Delta G_V^2}\left(2-\cos\Psi+\cos^3\Psi\right). \tag{2}$$

Experimental data allow calculating ΔG^*. We accept that the linear dimension of the interface is 200 nm and the number of precipitates on one of its surfaces is 45 (this agrees with our structural examination results). Then $N \approx 1.5 \times 10^{11}$ cm^{-2}. We accept $N_0 = 10^{15}$ cm^{-2} which corresponds to the atomic density in the {111} plane. Thus $\Delta G^* = 1.7 \times 10^{-12}$ erg at 1200 °C (1 erg = 10^{-7} J). According to literary data [18, 19] $\sigma_{\alpha\theta} = 360 \div 500$ erg/cm^2. Accepting $\sigma_{\alpha\theta} = 400$ erg/cm^2 and $\Psi = 60°$ one can calculate ΔG_V: $\Delta G_V = -9.9 \times 10^{10}$ erg/cm^3 (-9.9 kJ/cm^3).

We will now calculate the change in the the Gibbs free energy of the system for precipitate nucleation by a homogeneous mechanism as seems to be the case for precipitate nucleation during annealing of Cz silicon. ΔG_V can be estimated by analogy with the Gibbs free energy estimation for solid phase precipitate nucleation during crystallization of a single-component liquid at its crystallization temperature T_{cr}. Then, according to an earlier work [20] the advantage in the free energy per molar volume of the solid phase is

$$\Delta G_V^{\text{er}} = -\frac{1}{\Omega}\frac{L_{\text{m}}}{T_{\text{m}}}\left(1-\frac{T_{\text{cr}}}{T_{\text{m}}}\right), \tag{3}$$

where Ω is the molar volume of the solid phase, L_{m} is the melting heat and T_{m} is the melting point. For Cz silicon the advantage in the Gibbs free energy for oxygen precipitate nucleation ΔG_V will be described by the formula

$$\Delta G_V = -\frac{1}{\upsilon^*}\frac{Q}{T_{\text{m}}}\left(1-\frac{T_{\text{nucl}}}{T_{\text{m}}}\right) \tag{4}$$

where Q is the heat of oxygen dissolution in silicon, T_{nucl} is the precipitate nucleation and growth temperature, T_{m} is the silicon melting point, υ^* is the volume occupied by one oxygen atom in a SiO_2 precipitate, $\upsilon^* \approx 2/3\Omega_{\text{Si}} = 3.76 \times 10^{-23}$ cm^3/at and Ω_{Si} is the volume per one atom in pure silicon. According to an earlier work [18], $Q = 16.53 \times 10^{-13}$ erg/at (99.54 kJ/mol). Calculations showed that for homogeneous SiO_2 precipitate nucleation (for simplicity we will accept that only a single type of oxygen precipitate forms in layers implanted with solely oxygen ions) at 700 °C $\Delta G_V = -1.74 \times 10^{10}$ erg/cm^2, and at 800 °C $\Delta G_V = -1.5 \times 10^{10}$ erg/cm^2. Thus for heterogeneous precipitate nucleation (carbon implantation) the change in the Gibbs free energy of the system is far greater than that for homogeneous oxygen precipitate nucleation in Cz silicon, $G_{V\text{hom}} = -(1.5 \div 1.74)^{10}$ erg/cm^3 and $\Delta G_{V\text{het}} = -9.9 \times 10^{10}$ erg/cm^3.

Experiments show that high-temperature annealing of oxygen ion doped layers produces precipitate-dislocation complexes that are typical of oxygen. The absence of nucleation centers suggests that these complexes form by a homogeneous mechanism. To check this one should first theoretically confirm that the heat treatment time chosen is sufficient for the formation of the experimentally observed density of defects. During annealing the precipitates grow by enlargement of existing nuclei, but new ones may also form. During the decomposition of a supersaturated solid solution the concentration of precipitates N tends to a certain limit N_{s} determined by a decrease of the chemical driving force of transformation and a decrease of the second phase nucleation rate. We denote the time required for N to reach N_{s} as t_{s}. It is well-known [21] that N_{s} and t_{s} can be calculated using the following semi-empirical expressions:

$$N_{\text{s}} = I_0^{3/5}\left(\frac{4}{3}\pi D_{\text{O}}^{3/2}\right)^{-2/5}; \tag{5}$$

$$t_{\text{s}} = \left(\frac{4}{3}\pi D_{\text{O}}^{3/2} I_0\right)^{-2/5}, \tag{6}$$

where I_0 is the nucleation rate and D_{O} is the oxygen diffusion coefficient in silicon at the precipitate nucleation and growth temperature. For a homogeneous mechanism the SiO_2 nucleation rate is described as follows [18]:

$$I_0 = 4\pi Z\frac{D_{\text{O}}}{d}c_{\text{O}}^2 r_{\text{c}}^2\exp\left(-\frac{4\pi\sigma_{\alpha\theta}r_{\text{c}}^2}{3kT}\right)\exp\left(-\frac{t}{\tau}\right), \tag{7}$$

Table 1. Parameters of the process of precipitate formation by a homogeneous mechanism at various of silicon oxygen supersaturation degrees.

c_O, 10^{18} cm^{-3}	T_e, K	$(T_e - T_0)/T_e$	ΔG_V, 10^{10} erg/cm^3	r_c, 10^{-8} cm	I_0, cm$^{-3}\cdot$ c^{-1}	N_s, cm^{-3}	t_s, c
4.4	–	–	–	–	8.42	10^6	118.74×10^3
5	2092.76	0.296	-1.220	6.557	7.599×10^3	–	–
6	2161.758	0.319	-1.300	–	–	–	–
7	2223.845	0.338	-1.320	–	8.42×10^5	10^9	1187.4
8	2280.582	0.354	–	–	–	–	–
9	2333.087	0.369	–	–	–	–	–
10	2382.146	0.382	-1.572	5.087	2.445×10^{10}	5×10^{11}	–
20	2428.337	0.393	–	–	8.42×10^{10}	10^{12}	11.874

where Z is the Zeldovich factor, r_c is the critical precipitate radius, d is the interatomic distance and c_O is the initial concentration of oxygen in silicon. The precipitation rate *vs* time curve incorporates the incubation time τ of precipitate nucleation. It is commonly believed that this time is far shorter than the precipitate growth time t. The formula of the critical size of a spherical precipitate is as follows [22]:

$$r_c = \frac{2\sigma_{\alpha\theta}}{|\Delta G_V|}. \quad (8)$$

It is accepted in Eq. (7) that the surface tension is $\sigma_{\alpha\theta}$ = 400 erg/cm^2 and the Zeldovich factor is ≥ 0.001.

The nucleation parameters obtained from a calculation using the above formulae for different Si–O solid solution supersaturation degrees are summarized in Table 1. These data suggest that at 1200 °C it is possible to achieve a precipitate density of 10^9–10^{11} cm^{-3}. This requires oxygen concentrations of one and a half order of magnitude higher than the oxygen solubility in silicon at T = 1200 °C ($c_O^s = 4.81 \times 10^{17}$ cm^{-3}). These oxygen concentrations can be achieved at the oxygen implantation doses used in this experiment. (Note that in this case we mean that the oxygen concentration is the averaged oxygen concentration in the ion doped layer with a thickness of the order of $2\Delta R_p$, where ΔR_p is the struggling of the oxygen concentration profile). For example, for oxygen ion implantation at 300 eV and R_p = 0.68 μm, ΔR_p = 150÷170 nm which corresponds to an oxygen concentration of (5–6) × 10^{19} cm^{-3}. For these high supersaturation degrees Eq. (4) should be transformed to

$$\Delta G_V = -\frac{1}{\upsilon^*}\frac{Q}{T_e}\left(1 - \frac{T_0}{T_e}\right), \quad (9)$$

where T_0 is the temperature of precipitate formation, T_e is the temperature obtained by extrapolation of the oxygen solubility in silicon *vs* temperature curve (Eq. (10)) to above the melting point. The oxygen solubility in silicon was calculated using the formula [18]

$$c_O^s = 1.63 \cdot 10^{21} \exp\left(-\frac{99.54 \text{ kJ/mol}}{RT}\right), \quad (10)$$

where R is the universal gas constant.

Our calculations confirmed the assumed defect formation mechanism during annealing in the oxygen ion implanted layer. The calculated ΔG_V were close to those obtained by calculating the change in the Gibbs free energy for oxygen precipitation by a homogeneous mechanism in Cz silicon during annealing at T = 700 °C.

3.2 Implantation of two impurities

The correlated behavior of the carbon and oxygen diffusion fluxes allows us to use the Onsager theory [23, 24] for describing the uphill diffusion of carbon. According to Onsager the flow j of the i-th property depends linearly on all the thermodynamic forces acting in the system:

$$j_i = \sum_k L_{ik} X_k, \quad (11)$$

where L_{ik} is the kinetic coefficient and X_k is the generalized thermodynamic force. The matrix $|L_{ik}|$ of the kinetic coefficients contains the diagonal coefficients L_{ii} describing the effect of the thermodynamic force X_i on the flux of the intrinsic property j_i and the non-diagonal (crossing) coefficients L_{ik} ($i \neq k$) describing the effect of the thermodynamic force X_i on the flux of other properties. A fundamental standpoint of the Onsager theory is the equality of the kinetic coefficients $L_{ik} = L_{ki}$. Hereinafter when referring to the Onsager theory we will use the expression of X_k for a system without energy fluxes. Then the generalized driving force of the i-th element is written as $-\nabla\mu_k$, where μ_i is the chemical potential of any solution component. Therefore the formal expressions describing the mutual effects of the diffusn fluxes of the elements 1 and 2 dissolved in the matrix of the third element can be written as

$$j_1 = -L_{11}\nabla\mu_1 - L_{12}\nabla\mu_2; \quad (12a)$$

$$j_2 = -L_{21}\nabla\mu_1 - L_{22}\nabla\mu_2. \quad (12b)$$

The connection between the chemical potentials of the components in a solid solution (carbon and oxygen solution in silicon) is described by the Gibbs–Duhem equation [19]

$$c_1\nabla\mu_1 + c_2\nabla\mu_2 = 0, \quad (13)$$

where c_1 and c_2 are the concentrations of carbon and oxygen, respectively, in atomic fractions.

Set of Eqs (12) can be represented as follows:

$$j_1 = -L_{11}\nabla\mu_1\left(1 - \frac{c_1}{c_2}\frac{L_{12}}{L_{11}}\right); \quad (14a)$$

$$j_2 = -L_{22}\nabla\mu_2\left(1-\frac{c_2}{c_1}\frac{L_{12}}{L_{22}}\right). \qquad (14b)$$

The problem of the mutual effects of the diffusion fluxes can be simplified if one assumes that the diffusion of each of the components obeys Fick's law, by analogy with ideal solutions. Then the partial diffusion coefficient D_i can be represented through the kinetic coefficient L_{ii}

$$D_i = \frac{L_{ii}}{c_i}kT, \qquad (15)$$

where L_{ii}/c_i has the meaning of the mobility U_i. Thus, finally, set of Eqs (12) takes on

$$j_1 = -D_1^*\left(1-\frac{c_1}{c_2}\frac{L_{12}}{L_{11}}\right)\nabla c_1 = -D_1^{ef}\nabla c_1; \qquad (16a)$$

$$j_2 = -D_2^*\left(1-\frac{c_2}{c_1}\frac{L_{12}}{L_{22}}\right)\nabla c_2 = -D_2^{ef}\nabla c_2, \qquad (16b)$$

where D_1^{ef} and D_2^{ef} are the experimentally observed effective diffusion coefficients of the first and second solution components which become negative. It follows from Eqs (16) that uphill diffusion of both the first and the second solution components may occur if the second term in the parentheses is greater than 1. The experimentally revealed diffusion fluxes of carbon and oxygen toward the center of the ion doped layer suggest a strong mutual attraction of carbon and oxygen when the chemical forces (in the case considered these forces are the chemical interaction between oxygen and carbon) are far greater than the entropy contribution to the diffusion flux.

The above set of equations for diffusion fluxes does not allow for the diffusion fluxes of matrix atoms but this is justified for interstitial diffusion. Oxygen diffuses in silicon by an interstitial mechanism and hence the Onsager expression for the diffusion flux is completely correct for this element. Structural studies carried out in this work show that carbon implanted into silicon is in interstitial positions. Therefore the relatively formal Onsager approach is correct in this case. Structural studies of ion doped silicon layers in which carbon and oxygen ions were consistently implanted with doses of 0.6×10^{15} and 2.4×10^{15} 1/cm^2 (the total dose is the same as for implantation of solely carbon ions) showed that another type of structure forms in this case. The structure consists of perfect loops decorated with cluster-like features, with the loop density increasing closer to R_p. The optimum carbon and oxygen ion dose ratio for this defect formation mechanism is 1 : 4. The formation of a defect structure in the ion doped oxygen and carbon layers is strongly affected by the chemical carbon-oxygen bond. This bond is so strong that intrinsic silicon interstitial atoms cannot participate in the formation of cluster-like agglomerations of carbon and oxygen atoms. Instead interstitial silicon atoms form the perfect loops observed.

It follows from the above that the presence of a large number of dislocation loops, the sharp localization of the damaged region and the absence of diffusion smearing of the damaged region at device process annealing steps are quite favorable for efficient gettering. Indeed, studies of epitaxial films grown on substrates after different implantation versions showed that the defect density in the epitaxial films grown on the reference substrates was $(8–9) \times 10^3–5 \times 10^4$ cm^{-2}. For implantation of sole oxygen there was a weakly resolved layer of discrete defects under the epitaxial film, and the defect etching pattern in the film differed but slightly from that for the epitaxial films

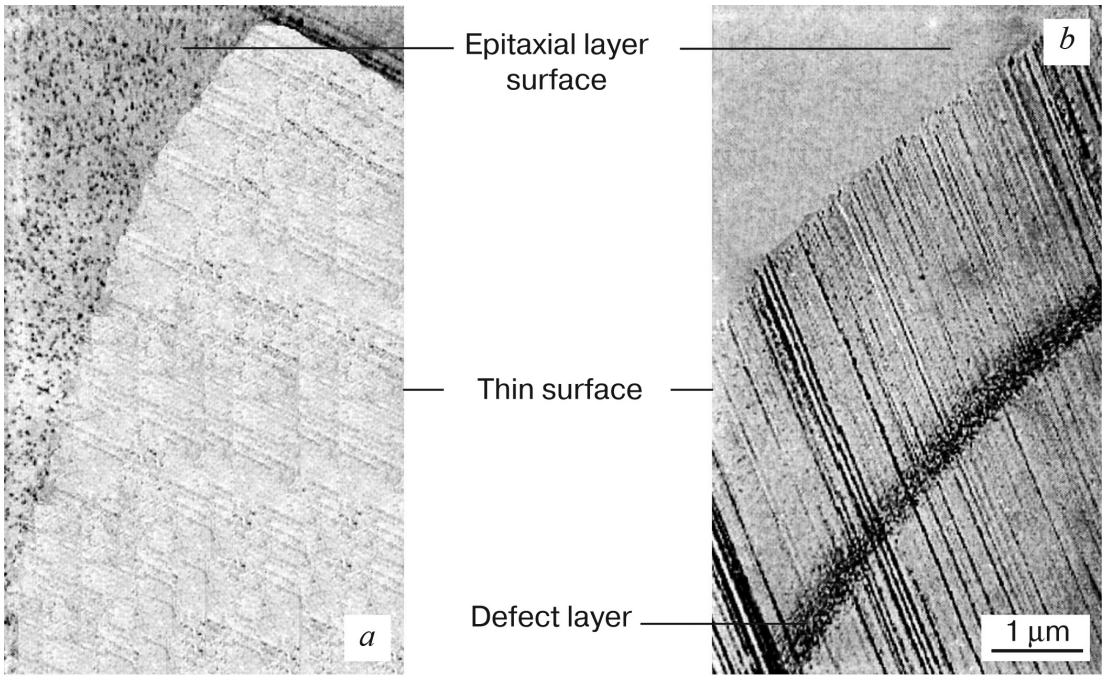

Figure 7. Micrographs of spherical cross-sections of epitaxial structures on substrates (*a*) without ion doping and (*b*) after preliminary implantation of C ions at a carbon to oxygen ion dose ratio of 1 : 4.

grown on the reference substrates. The best result was obtained for implantation of two impurities at a 1 : 4 dose ratio. Then the defect density in the film was 1×10 cm^{-2}, and the surface layer under the film had a clearly seen narrow layer of gettering centers (Fig. 7).

4. Conclusion

Analysis of the gettering properties of silicon layers implanted with C and O ions from the standpoints of the thermodynamics and kinetics of the processes occurring there during annealing revealed the following:

– if the layer is implanted with sole carbon, then carbon does not occupy silicon lattice site during annealing, unlike boron, but forms defects of a special type;
– the presence of uphill diffusion in the layers after double implantation with carbon and oxygen ensures the absence of diffusion smearing of the layers during long-term annealing and leads to the formation of a large number of dislocation loops thus making these layers optimal for the formation of efficient gettering regions.

References

1. Abe H., Yamamoto S., Miyashita A., Siskafus K.E. Formation mechanisms for carbon onions and nanocapsules in C^+-ion implanted copper. *J. App. Phys.*, 2001; 90(7): 3353–3358. https://doi.org/10.1063/1.1402143
2. Abe H. Nucleation of carbon onions and nanocapsules under ion implantation at high temperature. *Diamond and Related Mater.*, 2001; 10(3–7): 1201–1204. https://doi.org/10.1016/S0925-9635(00)00452-0
3. Thune E., Cabioc'h T., Guérin Ph., Denanot M.-F., Jaouen M. Nucleation and growth of carbon onions synthesized by ion-implantation: a transmission electron microscopy study. *Mater. Lett.*, 2002; 54(2–3): 222–228. https://doi.org/10.1016/S0167-577X(01)00567-5
4. Skorupa W., Kögler R., Schmalz K., Bartsch H. Proximity getterihg by MeV-implantation of carbon: microstructure and carrier lifetime measurements. *Nuclear Instruments and Meth. in Phys. Res. B*, 1991; 55(1–4): 224–229. https://doi.org/10.1016/0168-583X(91)96167-J
5. Pilipenko V.A., Gorushko V.A., Petlitskiy A.N., Ponaryadov V.V., Turtsevich A.S., Shvedov S.V. Methods and mechanisms of gettering of silicon structures in the production of integrated circuits. *Tekhnologiya i Konstruirovanie v Elektronnoi Apparature*, 2013; (2–3): 43–57. (In Russ.)
6. Skorupa W., Kögler R., Schmalz K., Gaworzewski P., Morgenstern G., Syhre H. Iron gettering and doping in silicon due to MeV carbon implantation. *Nuclear Instruments and Meth. in Phys. Res. B*, 1993; 74(1–2): 70–74. https://doi.org/10.1016/0168-583X(93)95016-X
7. Aleshin A.N., Enisherlova K.L., Kalinin A.A., Mordkovich V.N. The chemical factor and its influence on the formation of defect structures and their gettering properties in layers of silicon implanted with chemical-active ions. *Nuclear Instruments and Meth. in Phys. Res. B*, 1996; 112(1–4): 184–187. https://doi.org/10.1016/0168-583X(95)01247-8
8. Aleshin A.N., Enisherlova K.L., Kalinin A.A., Mordkovich V.N., Rusak T.F. Creation of an internal getter in silicon by implantation of carbon and oxygen ions. *Poverkhnost'*, 1992; (1): 35–40. (In Russ.)
9. Burenkov A.F., Komarov F.F., Kumakhov M.A., Temkin M.M. *Tablitsy parametrov prostranstvennogo raspredeleniya ionnoimplantirovannykh primesei* [Tables of spatial distribution parameters of ion implanted impurities]. Minsk: Izd-vo BGU im. Lenina, 1980, 348 p. (In Russ.)
10. Mordkovich V.N., Sukhodreva I.M., Cheryukanova L.D. Deformation profiles in implanted gallium arsenide layers. *Poverkhnost'*, 1983; (4): 90–95. (In Russ.)
11. Enisherlova K.L., Italyantsev A.G., Tkacheva T.M. The termodynamical model of the internal guttering in Si. *Proc. 11 Sci. and Business Conf. «SILICON 2008»*. Rožnov pod Radhoštěm (Czech Republic): TECON Scientific, 2008: 257–271.
12. Newman R.C. Light impurities and their interactions in silicon. *In European Materials Research Society Symposia Proceedings. C, H, N and O in Si and Characterization and Simulation of Materials and Processes*, 1996: 1–12. https://doi.org/10.1016/B978-0-444-82413-4.50008-1
13. Komarov F.F., Novikov A.P., Soloviev V.S., Shiryaev S.Yu. *Defekty struktury v implantirovannom kremnii* [Structural defects in implanted silicon]. Minsk, 1990: 21–47. (In Russ.)
14. Tamura M. Secondary defects in phosphorus-implanted silicon. *Appl. Phys. Lett.*, 1973; 23(12): 615–653. https://doi.org/10.1063/1.1654779
15. Piskunov D.I. Electron microscopic studies of the nature of defects arising from post-implantation annealing of silicon. Dis. Cand. Sci. (Phys.-Math.). Moscow, 1977. (In Russ.)
16. *Fizicheskie velichiny: Spravochnik* [Physical quantities]. Moscow: Energoatomizdat, 1991, 1232 p. (In Russ.)
17. Yin Y.F., Faulkner R.G. Modelling the effects of alloying elements on precipitation in ferritic steels. *Materials Science and Engineering: A,* 2003; 344(1–2): 92–102. https://doi.org/10.1016/S0921-5093(02)00418-5
18. Yang K., Carle J., Kleinhenz R. Formation of the oxygen precipitate-free zone in silicon. *J. Appl. Phys.*, 1987; 62(12): 4890–4896. https://doi.org/10.1063/1.338996
19. Italyantsev A.G. Basic processes accompanying solid-phase reactions on the silicon surface. *J. Appl. Phys.*, 1996; 79(5): 2369–2375. https://doi.org/10.1063/1.361164
20. Zhukhovitsky A.A., Shvartsman L.A. *Fizicheskaya khimiya* [Physical chemistry]. Moscow: Metallurgy, 1987, 688 p. (In Russ.)
21. Aleshin A. N. Features of the kinetics of the second phase in supersaturated silicon layers implanted with oxygen. *Poverkhnost'*, 1989; (10): 109–116. (In Russ.)
22. Kelton K.F., Falster R., Gambaro D., Olmo M., Cornara M., Wei P.F. Oxygen precipitation in silicon: Experimental studies and theoretical investigations within the classical theory of nucleation. *J. Appl. Phys.*, 1999; 85(12): 8097–8105. https://doi.org/10.1063/1.370648
23. Bokshtein B.S., Mendeleev M.I. *Kratkii kurs fizicheskoi khimii* [Short course of physical chemistry]. Moscow: CheRo, 2001, 232 p.
24. Kuni F.M., Shchekin A.K., Novozhilova T. Yu.Onsager reciprocal relations in nonequilibrium thermodynamics. *Vestnik sankt-peterburgskogo universiteta. Fizika i khimiya*, 2005; (3): 125–129. (In Russ.)